Electronic Supplementary Material (ESI) for Materials Advances.

Ambient-Pressure Ozone Treatment Enables Tuning of Oxygen Vacancy Concentration in the $La_{1-x}Sr_xFeO_{3-\delta}$ ($0 \leq x \leq 1$) Perovskite Oxides

Geletu Qing,[1] David Thompson,[1] Mourad Benamara,[2] Clemens Heske,[3,4] Lauren Greenlee,[5,*] Jingyi Chen[1,*]

[1]Department of Chemistry and Biochemistry, University of Arkansas, Fayetteville

[2]Institute of Nanoscience and Engineering, University of Arkansas, Fayetteville

[3]Department of Chemistry and Biochemistry, University of Nevada, Las Vegas

[4]Institute for Photon Science and Synchrotron Radiation (IPS) and Institute for Chemical Technology and Polymer Chemistry (ITCP), Karlsruhe Institute of Technology (KIT), Karlsruhe, Germany

[5]Department of Chemical Engineering, Pennsylvania State University

Corresponding authors: Jingyi Chen (chenj@uark.edu); Lauren Greenlee (greenlee@psu.edu)

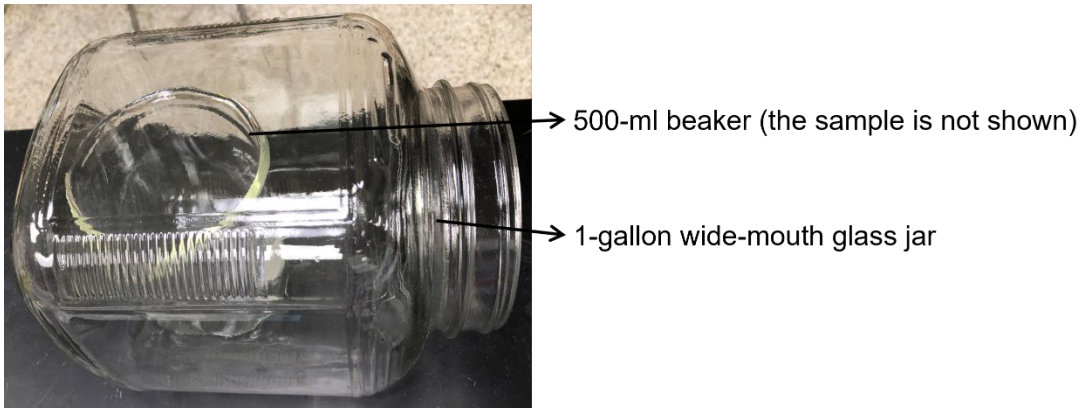

Figure S1. Experimental setup for heating the gelled samples at 200 °C. The beaker containing a gelled sample is placed in a 1-gallon wide-mouth glass jar, which is then placed inside the furnace chamber. The gelled sample is not shown in the photograph. After the heat treatment is completed, the sample powder is collected from the beaker and the glass jar.

Figure S2. Experimental setup for the ozone treatment.

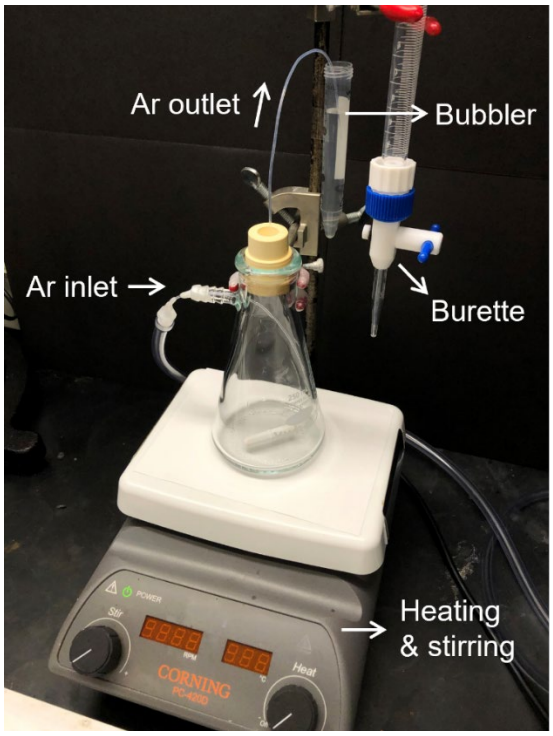

Figure S3. Experimental setup for redox titration. A Teflon tube is used for Ar purging, sealed to the sidearm of the filtering flask using Parafilm. The Teflon tube inside the flask can be raised by pulling it from the other end to switch from purging to sweeping above the solution surface. The rubber septum is removed when chemicals are added to the flask.

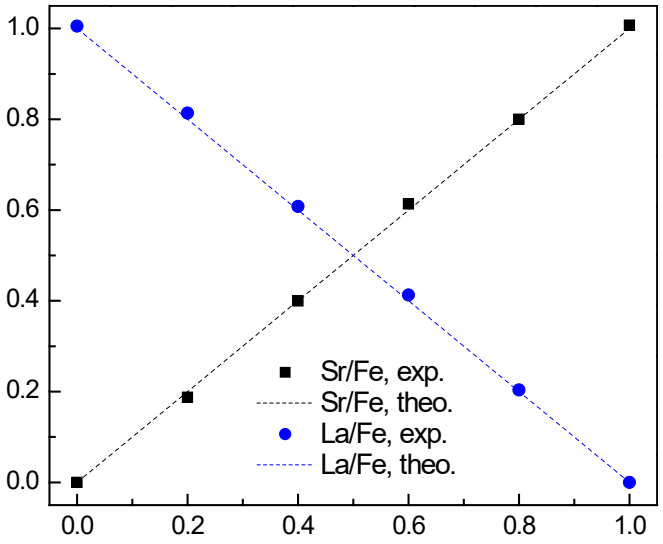

Figure S4. Elemental composition of the $La_{1-x}Sr_xFeO_{3-\delta}$ compounds, obtained from ICP-MS measurements (black and blue symbols), versus the theoretical values of x (dashed lines, "Sr/Fe, theo." and "La/Fe, theo."). All theoretical values are calculated based on the molar ratios of the La, Sr, and Fe precursors used for the synthesis of each sample.

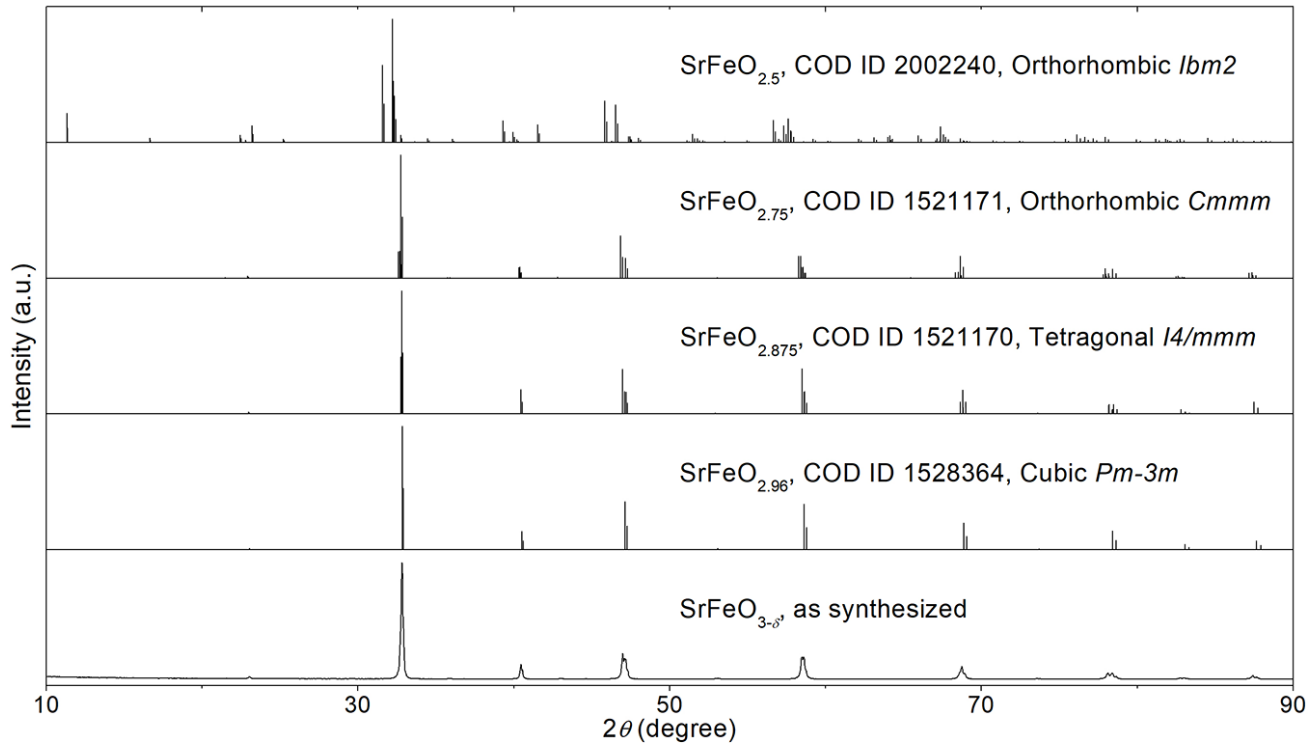

Figure S5. (a) Comparison of the XRD pattern of the as-synthesized $SrFeO_{3-\delta}$ compound without ozone treatment and the calculated patterns for $SrFeO_{2.96}$ (COD ID 1528364, Cubic *Pm-3m*), $SrFeO_{2.875}$ (COD ID 1521170, Tetragonal *I4/mmm*), $SrFeO_{2.75}$ (COD ID 1521171, Orthorhombic *Cmmm*), and $SrFeO_{2.5}$ (COD ID 2002240, Orthorhombic *Ibm2*). The calculated patterns were generated using the VESTA software and the Crystallographic Information Files (CIF) obtained from the Crystallography Open Database (COD).[1-7]

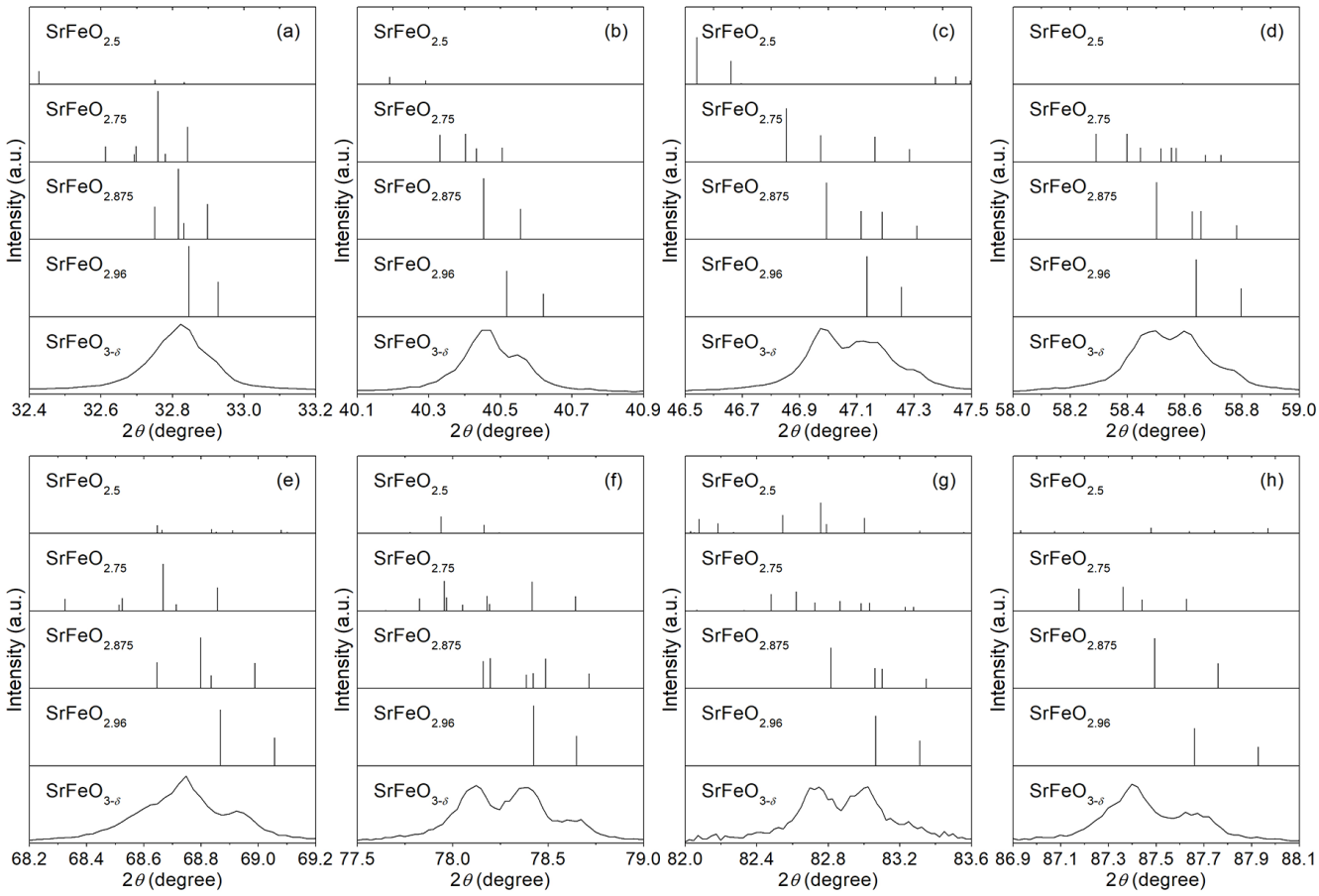

Figure S6. (a-h) Zoom-in regions of the XRD patterns in Figure S5. It can be seen that the XRD pattern of the as-synthesized $SrFeO_{3-\delta}$ compound is significantly different from the calculated pattern for $SrFeO_{2.5}$. Furthermore, most of the diffraction peaks for the as-synthesized $SrFeO_{3-\delta}$ compound are composed of more than two peaks, which do not match the doublets observed in the calculated pattern for $SrFeO_{2.96}$. Therefore, the models of $SrFeO_{2.5}$ (orthorhombic, *Ibm2*) and $SrFeO_{2.96}$ (cubic, space group *Pm-3m*) were ruled out, which is also evidenced by the Rietveld refinement: the experimental data could not be fit using these models. The similarities between the XRD pattern of the as-synthesized $SrFeO_{3-\delta}$ compound and the calculated patterns for $SrFeO_{2.75}$ and $SrFeO_{2.875}$ indicate that the as-synthesized $SrFeO_{3-\delta}$ compound may have a crystalline structure similar to that of $SrFeO_{2.75}$ or $SrFeO_{2.875}$.

Rietveld refinement showed a reasonable agreement between the experimental data and the calculated patterns obtained using the models of $SrFeO_{2.875}$ (tetragonal, space group *I4/mmm*) and $SrFeO_{2.75}$ (orthorhombic, space group *Cmmm*), achieving goodness-of-fit (χ^2) values of 1.47 and 1.52, respectively. However, the Fe-O bond distances obtained from the refinement based on the model of $SrFeO_{2.875}$ (tetragonal, space group *I4/mmm*) showed the presence of an unaccountably short Fe-O bond, *d*(Fe-O) = 1.7741 Å, indicating that this is not the correct model (the shortest Fe-O bonds typically observed in mixed alkaline-earth iron oxide compounds are about 1.85 Å).[8] Based on these analyses, the major phase in the $SrFeO_{3-\delta}$ compound after calcination at 1,300 °C is identified to be $SrFeO_{2.75}$ (orthorhombic, space group *Cmmm*). However, it is highly likely that $SrFeO_{2.875}$ (tetragonal, space group *I4/mmm*) is also present in the compound as a minor phase, for the following reasons: (1) our redox titration showed an oxygen stoichiometry of 2.805 for the $SrFeO_{3-\delta}$ compound after calcination at 1,300 °C (see the Section 3.1 in the main text); (2) it was reported that $SrFeO_{2.75}$ (orthorhombic, space group *Cmmm*) and $SrFeO_{2.875}$ (tetragonal, space group *I4/mmm*) can coexist in $SrFeO_{2.80}$.[9]

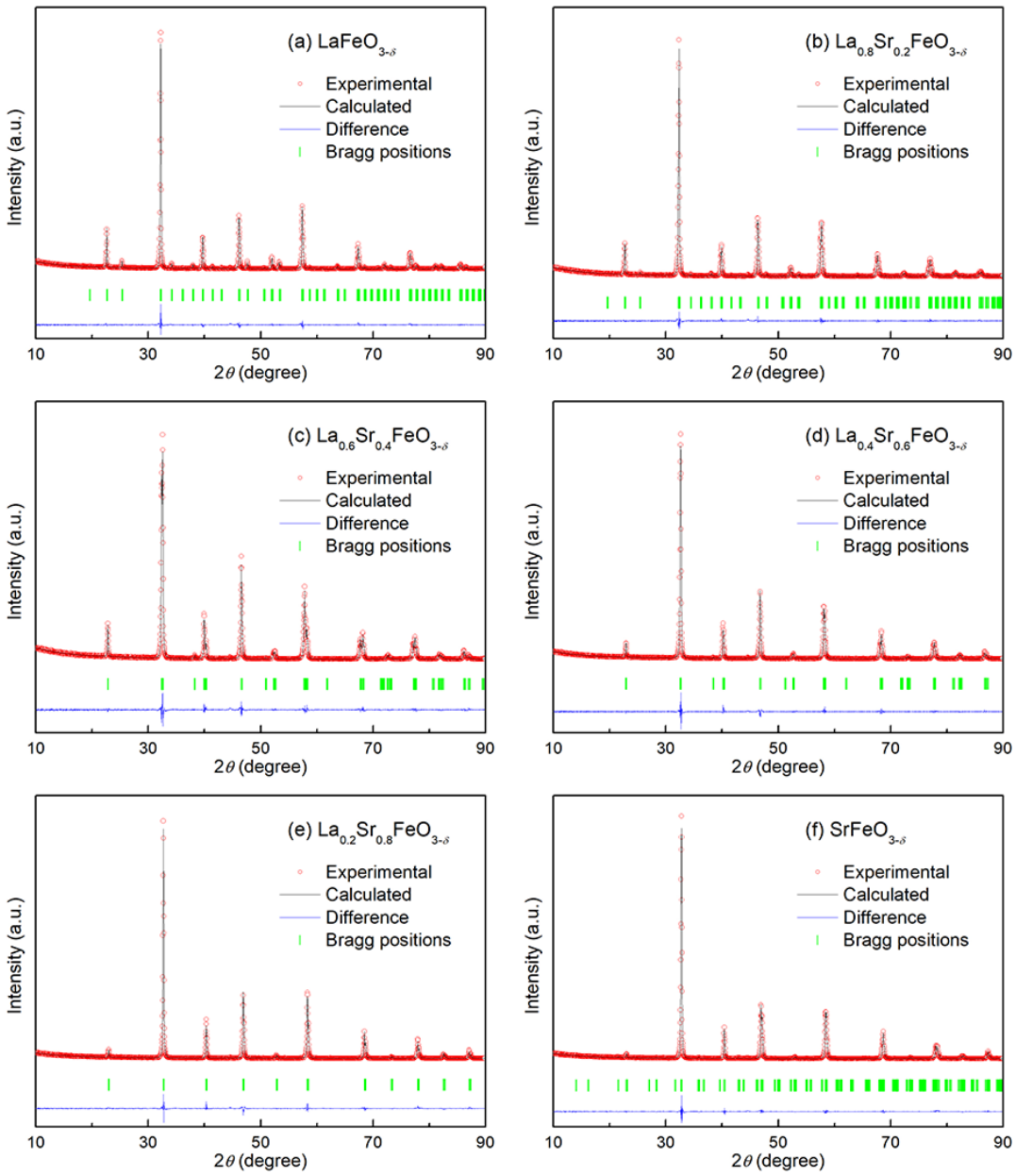

Figure S7. Rietveld refinement of the structural models for the $La_{1-x}Sr_xFeO_{3-\delta}$ compounds. The red dots are the experimental data points, and the black curves are the calculated XRD patterns. The difference between the experimental data points and the calculated XRD patterns is shown in blue curves. Bragg reflections are indicated using green vertical lines. *Note*: the region between 44° and 45.2° was excluded from the fitting because a diffraction peak of the aluminum sample plate is present in this region.

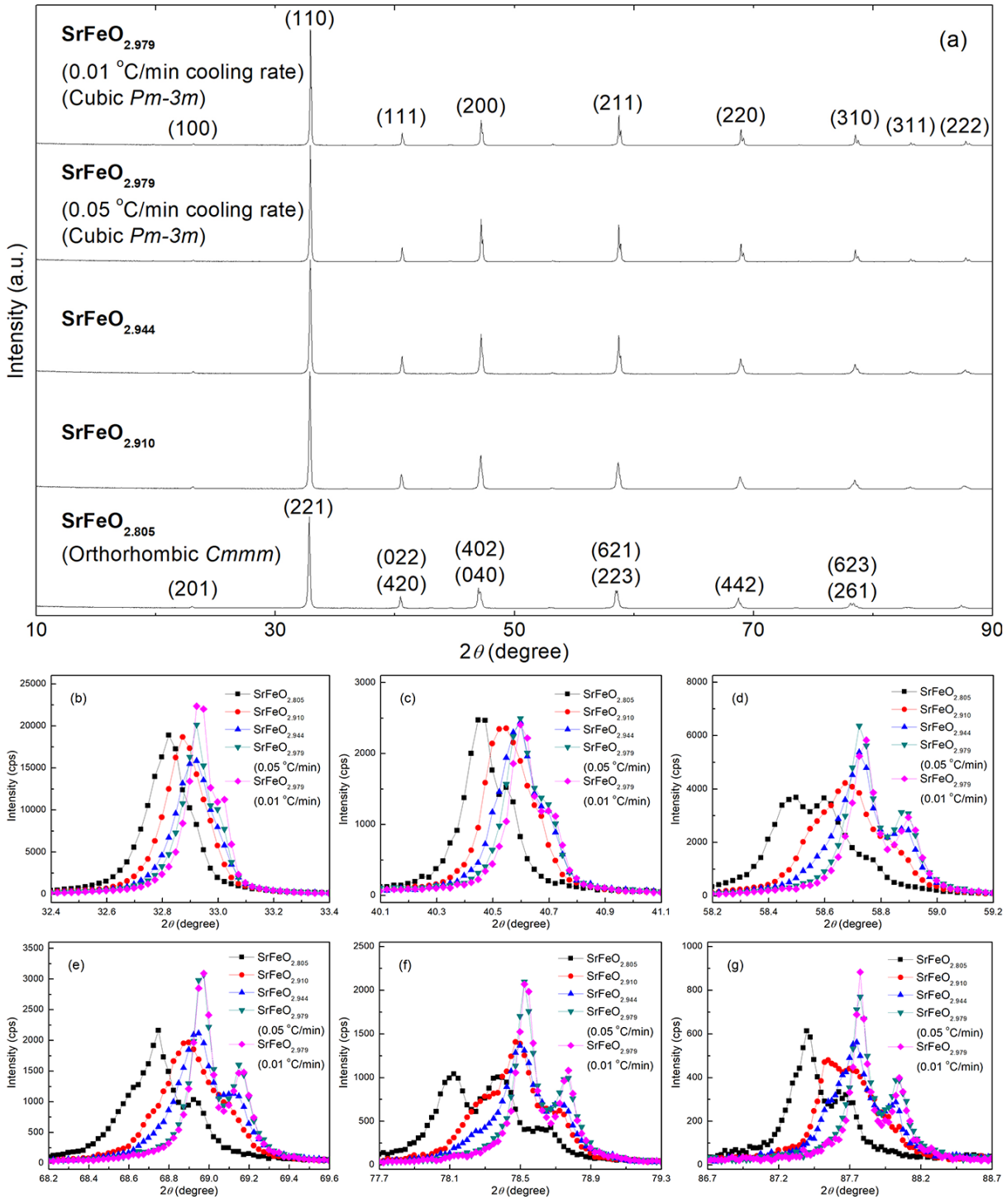

Figure S8. Effect of ozone treatment on the powder X-ray diffraction patterns of the $SrFeO_{3-\delta}$ compounds. (a) Full-range diffraction patterns and (b-g) enlarged regions of the major diffraction peaks.

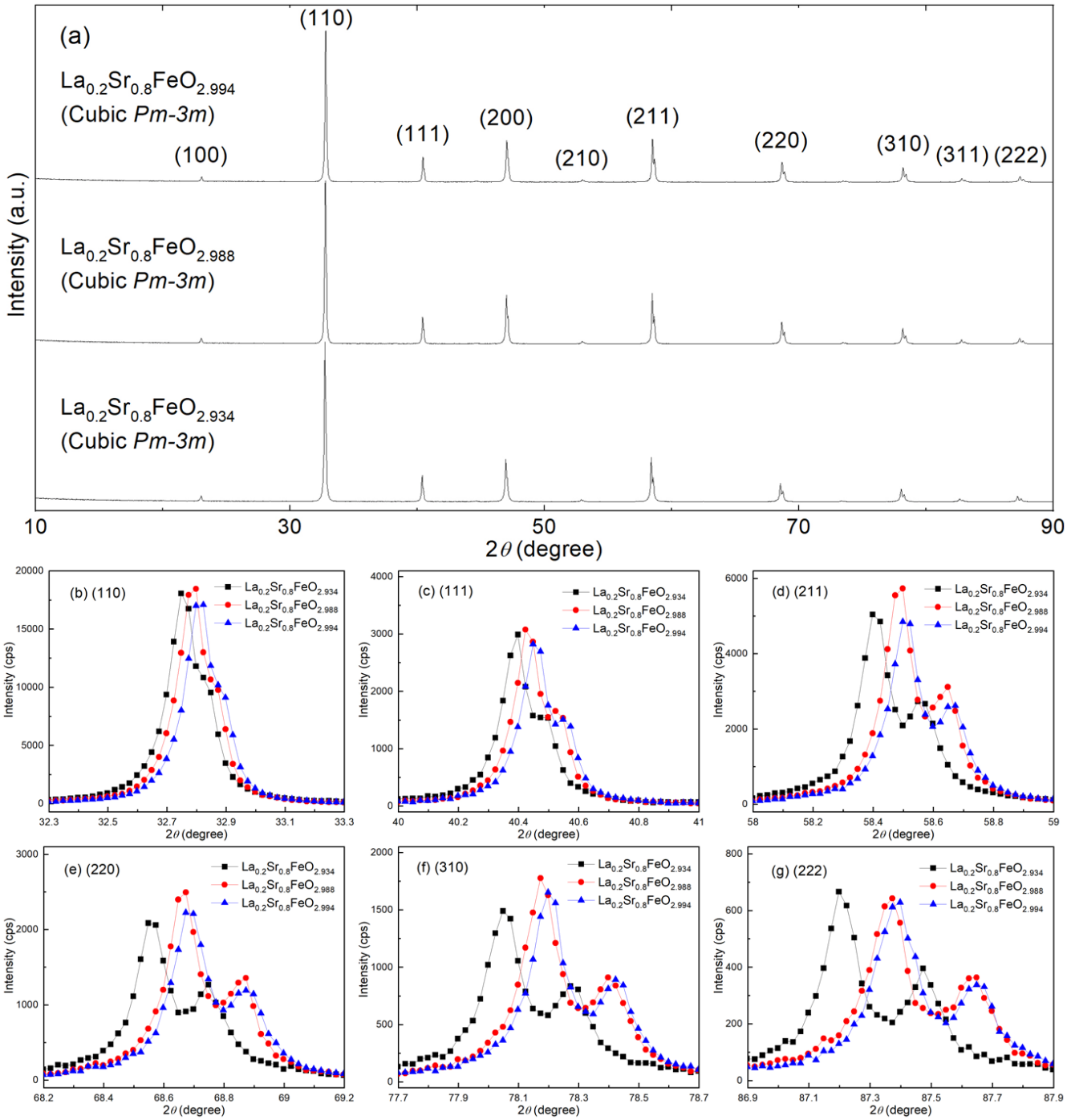

Figure S9. Effect of ozone treatment on the powder X-ray diffraction patterns of the $La_{0.2}Sr_{0.8}FeO_{3-\delta}$ compounds. (a) Full-range diffraction patterns and (b-g) enlarged regions of the major diffraction peaks.

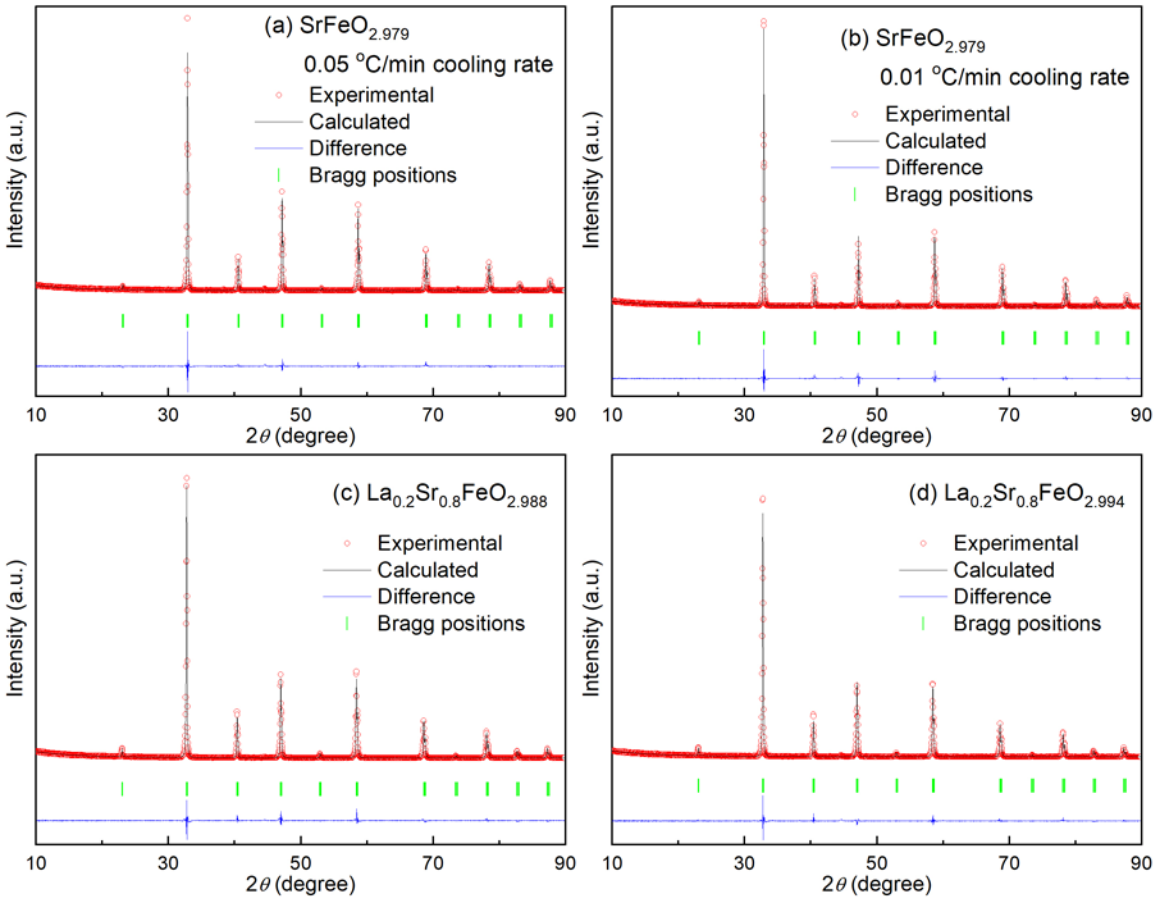

Figure S10. Rietveld refinement of the structural models for the ozone-treated (a,b) $SrFeO_{3-\delta}$ and (c,d) $La_{0.2}Sr_{0.8}FeO_{3-\delta}$ compounds. The red dots are the experimental data points, and the black curves are the calculated XRD patterns. The difference between the experimental data points and the calculated XRD patterns is shown as blue curves. Bragg reflections are indicated using green vertical lines. *Note*: the region between 44° and 45.2° was excluded from the fitting because a diffraction peak of the aluminum sample plate is present in this region.

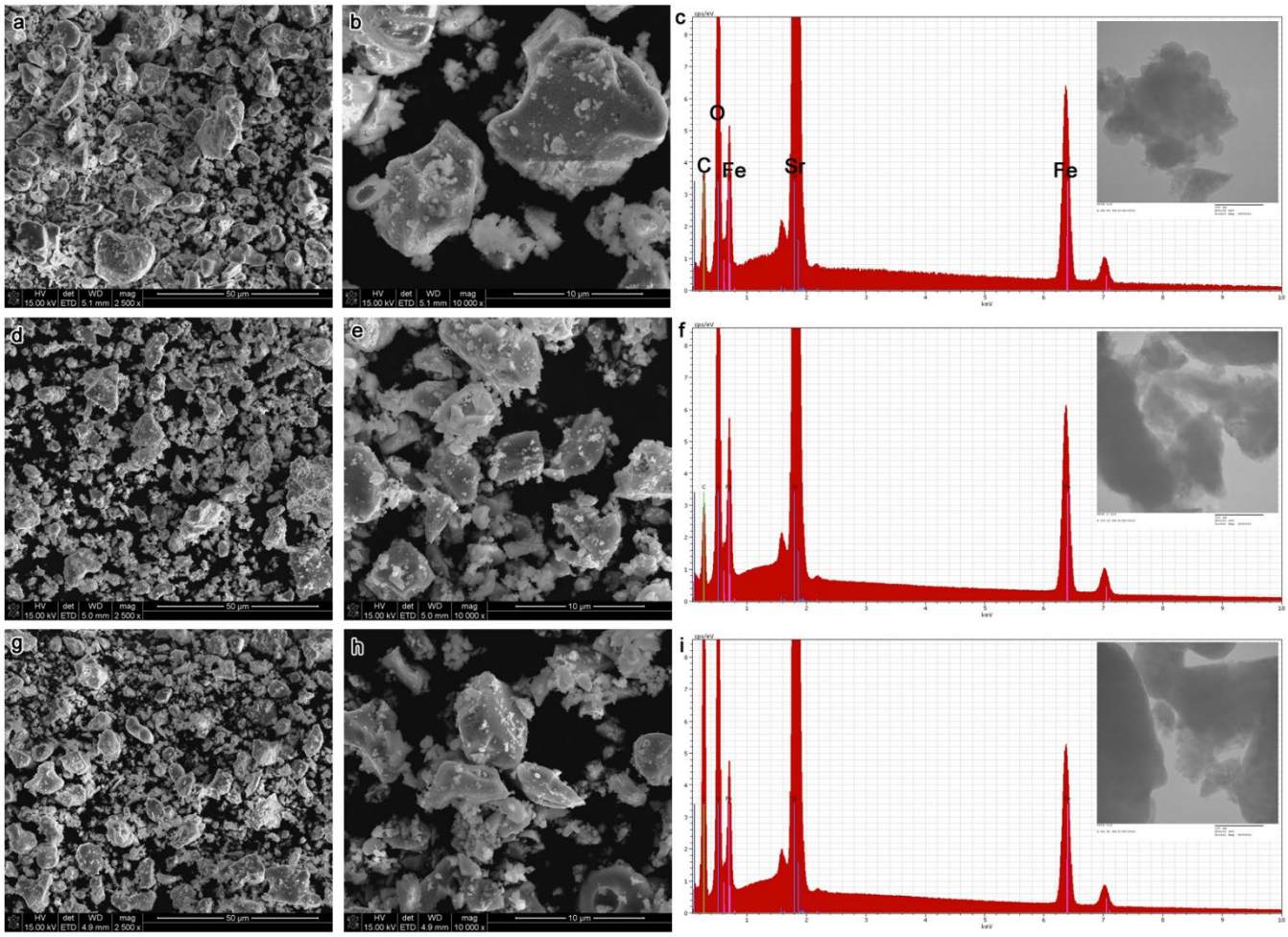

Figure S11. Electron microscopy characterization of the $SrFeO_{3-\delta}$ compound before and after ozone treatment. (a-c) SEM zoom-out, zoom-in images, and EDX spectrum of $SrFeO_{3-\delta}$ before ozone treatment. (d-f) SEM zoom-out, zoom-in images, and EDX spectrum of $SrFeO_{3-\delta}$ after ozone treatment at a cooling rate of 0.05 ºC/min. (g-i) SEM zoom-out, zoom-in images, and EDX spectrum of $SrFeO_{3-\delta}$ after ozone treatment at a cooling rate of 0.01 ºC/min. The scale bars of the SEM zoom-out and zoom-in images are 50 and 10 μm, respectively. The insets in (c), (f), and (i) are the TEM images of the corresponding samples (scale bar of 100 nm).

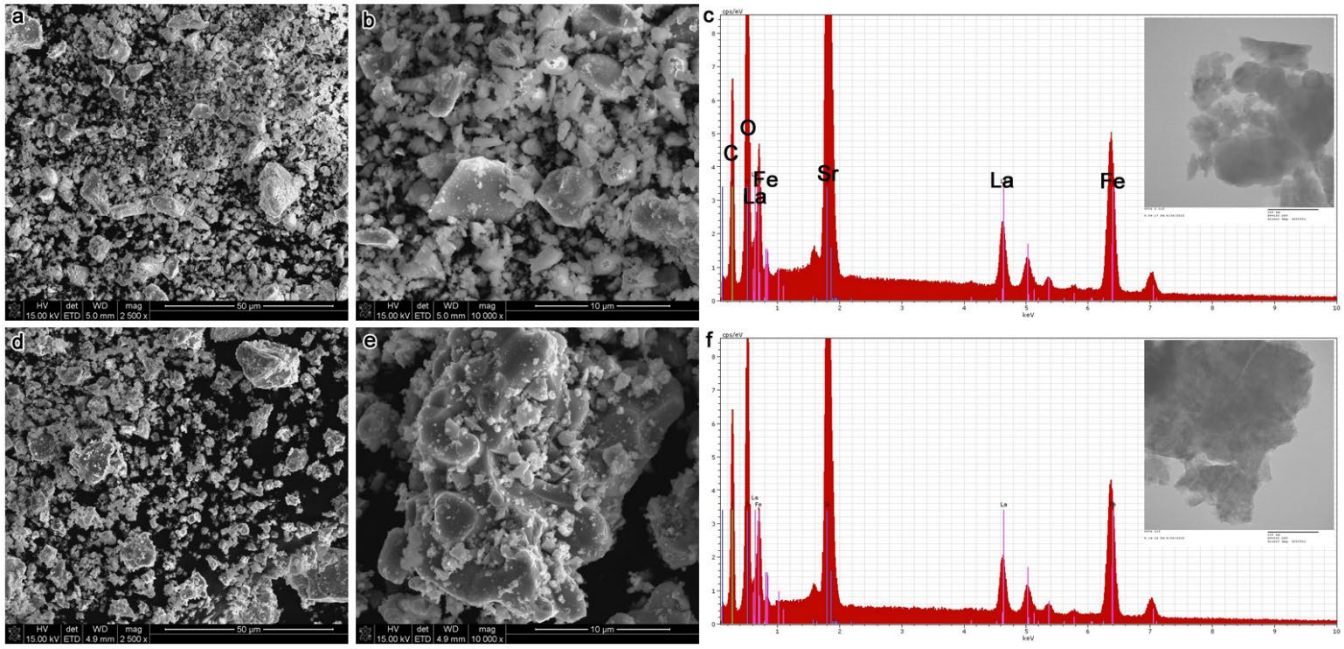

Figure S12. Electron microscopy characterization of the $La_{0.2}Sr_{0.8}FeO_{3-\delta}$ compound before and after ozone treatment. (a-c) SEM zoom-out, zoom-in images, and EDX spectrum of $La_{0.2}Sr_{0.8}FeO_{3-\delta}$ before ozone treatment. (d-f) SEM zoom-out, zoom-in images, and EDX spectrum of $La_{0.2}Sr_{0.8}FeO_{3-\delta}$ after ozone treatment at a cooling rate of 0.05 ºC/min. The scale bars of the SEM zoom-out and zoom-in images are 50 and 10 μm, respectively. The insets are the TEM images of the corresponding samples (scale bar of 100 nm).

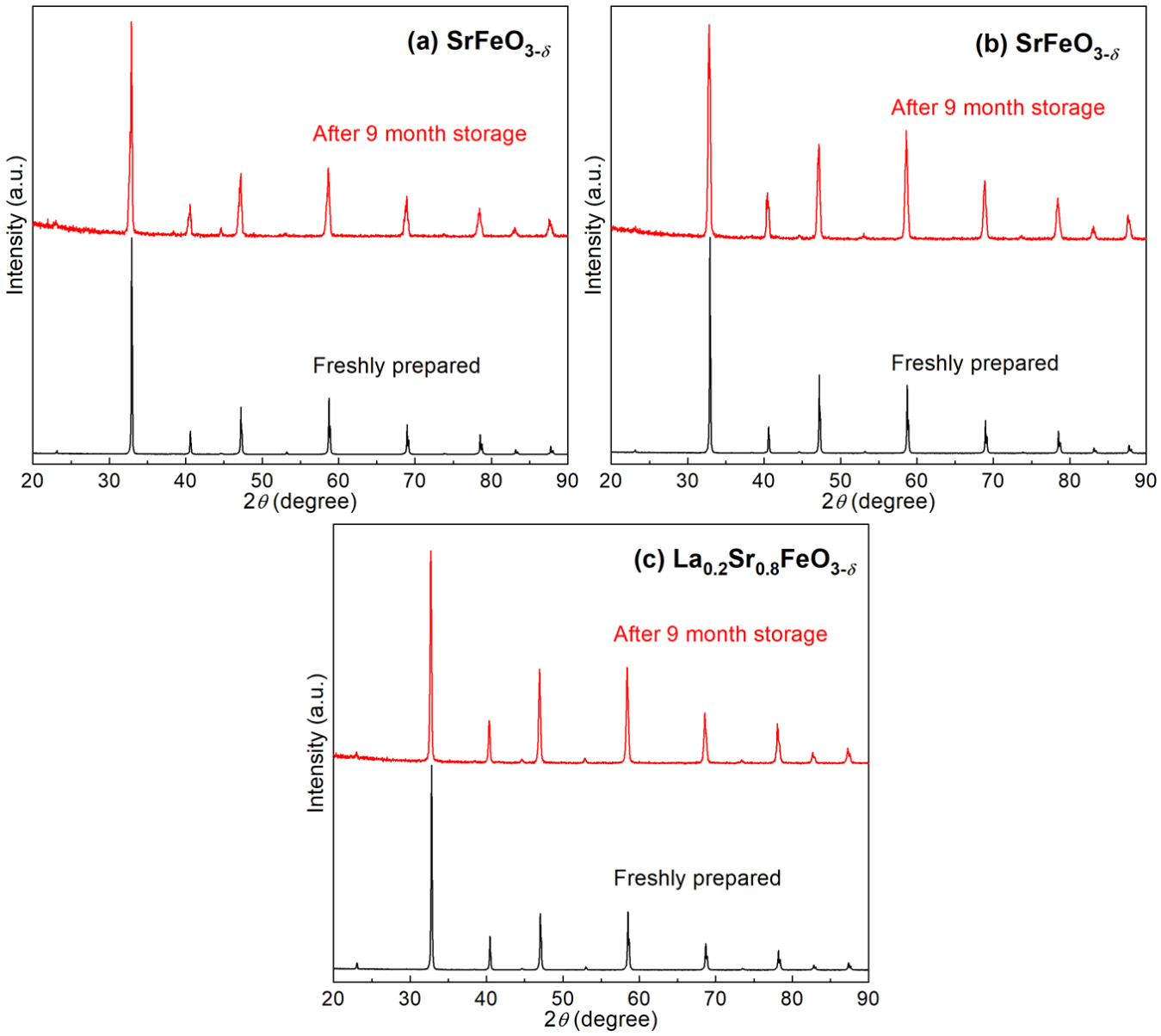

Figure S13. XRD characterization of the ozone-treated $SrFeO_{3-\delta}$ and $La_{0.2}Sr_{0.8}FeO_{3-\delta}$ compounds after 9 month storage under ambient condition, compared to the freshly prepared compounds: (a) ozone-treated $SrFeO_{3-\delta}$ at a cooling rate of 0.01 ºC/min; (b) ozone-treated $SrFeO_{3-\delta}$ at a cooling rate of 0.05 ºC/min; and (c) ozone-treated $La_{0.2}Sr_{0.8}FeO_{3-\delta}$ at a cooling rate of 0.05 ºC/min.

Table S1. Hot plate surface temperature and heating time required for the complete dissolution of the $La_{1-x}Sr_xFeO_{3-\delta}$ compounds and Fe_2O_3 in 6 M HCl.

Sample	$LaFeO_3$	$La_{0.8}Sr_{0.2}FeO_{3-\delta}$	$La_{0.6}Sr_{0.4}FeO_{3-\delta}$	$La_{0.4}Sr_{0.6}FeO_{3-\delta}$	$La_{0.2}Sr_{0.8}FeO_{3--\delta}$	$SrFeO_{3-\delta}$	Fe_2O_3
Temp. (°C)	270	270	270	180	120	RT	270
Time (min)	25	20	20	15	10	10	15

Notes: The temperature is the surface temperature of the hot plate, and the heating time includes the heating-up time from a cold hot plate to the designated temperature; these conditions may vary depending on the type of hot plate. Two sets of experiments were carried out to verify the accuracy of the titration method. First, the Mohr's salt was titrated with and without heating at 270 °C for 25 min, which corresponds to the highest temperature and longest heating time required for the complete dissolution of the $La_{1-x}Sr_xFeO_{3-\delta}$ compounds, as shown in **Table S1**. The mass of Fe(II) in the Mohr's salt was determined at 0.1459 ± 0.0001 and 0.1460 ± 0.0001 in the experiments with and without heating, respectively. This result indicates that the heating process had a negligible effect on the titration results. Second, the content of Fe(IV) in a commercially-available Fe_2O_3 compound was measured as a reference. The result yielded $y = -0.0008 \pm 0.0005$, as in $(Fe(III)_{1-y}Fe(IV)_y)_2O_3$, which agreed with the expected value ($y = 0$), i.e., no presence of Fe(IV). The titration of Fe_2O_3 was carried out on a weekly basis to validate the accuracy of the titration results.

Table S2. Effect of Sr content (x) on the concentrations of Fe(IV) (y) and oxygen vacancy (δ) in the as-synthesized $La_{1-x}Sr_xFe(III)_{1-y}Fe(IV)_yO_{3-\delta}$ compounds without ozone treatment. The values were determined from the titration results.

Sample (x)	0.0	0.2	0.4	0.6	0.8	1.0
y	0.012 ± 0.003	0.204 ± 0.001	0.395 ± 0.002	0.588 ± 0.003	0.667 ± 0.003	0.611 ± 0.002
δ	-0.006 ± 0.002	-0.002 ± 0.001	0.002 ± 0.001	0.006 ± 0.002	0.066 ± 0.002	0.195 ± 0.001

Table S3. Effect of ozone treatment conditions on the concentrations of Fe(IV) (y) and oxygen vacancies (δ) in the $SrFeO_{3-\delta}$ and $La_{0.2}Sr_{0.8}FeO_{3-\delta}$ compounds. The values were determined from the titration results.

Exp. No.	Temp. (°C)	Time (h)	Cooling rate (°C/min)	Opened furnace at (°C)	y	δ
1. $SrFe(III)_{1-y}Fe(IV)_yO_{3-\delta}$						
E1	200	2	N/A[a]	100[a]	0.819 ± 0.002	0.090 ± 0.001
E2	200	6	N/A[a]	100[a]	0.851 ± 0.002	0.074 ± 0.001
E3	225	6	N/A[a]	100[a]	0.887 ± 0.003	0.056 ± 0.001
E4	250	6	N/A[a]	100[a]	0.869 ± 0.005	0.065 ± 0.002
E5	275	6	N/A[a]	100[a]	0.866 ± 0.003	0.067 ± 0.001
E6	300	6	N/A[a]	100[a]	0.852 ± 0.005	0.074 ± 0.002
E7	400	6	N/A[a]	100[a]	0.846 ± 0.001	0.077 ± 0.001
E8	300	6	N/A[a]	150[a]	0.777 ± 0.003	0.111 ± 0.002
E9	300	6	N/A[a]	81[a]	0.891 ± 0.004	0.055 ± 0.002
E10	225	6	0.5	40[b]	0.950 ± 0.001	0.025 ± 0.001
E11	225	6	0.05	25[b]	0.957 ± 0.002	0.021 ± 0.001
E11 sample (after 9 month storage in a vial at room temperature)					0.939 ± 0.007	0.030 ± 0.002
E12	225	6	0.01	25[b]	0.958 ± 0.004	0.021 ± 0.002
E12 sample (after 9 month storage in a vial at room temperature)					0.950 ± 0.002	0.025 ± 0.001
2. $La_{0.2}Sr_{0.8}Fe(III)_{1-y}Fe(IV)_yO_{3-\delta}$						
E13	200	2	N/A[a]	100[a]	0.777 ± 0.002	0.012 ± 0.001
E14	225	6	0.5	40[b]	0.784 ± 0.004	0.008 ± 0.002
E15	225	6	0.05	25[b]	0.789 ± 0.001	0.006 ± 0.001
E15 sample (after 9 month storage in a vial at room temperature)					0.777 ± 0.004	0.012± 0.002

[a]After the 6 h ozone treatment, the furnace was turned off and the sample was allowed to cool down naturally under the ozone environment. The furnace was opened once the chamber temperature reached the values shown in the table. The quartz tube was then raised above the furnace chamber to allow for fast cooling. Once the temperature at the outer surface of the quartz tube reached room temperature, the ozone flow was stopped, and the sample was removed from the quartz tube. [b]These values indicate the furnace chamber temperature when the furnace program temperature reached 25 °C at the cooling rates specified in the table.

References

1. Vaitkus, A.; Merkys, A.; Grazulis, S., Validation of the Crystallography Open Database Using the Crystallographic Information Framework. *J. Appl. Crystallogr.* **2021**, *54*, 661-672.
2. Grazulis, S.; Merkys, A.; Vaitkus, A.; Okulic-Kazarinas, M., Computing Stoichiometric Molecular Composition from Crystal Structures. *J. Appl. Crystallogr.* **2015**, *48*, 85-91.
3. Grazulis, S.; Daskevic, A.; Merkys, A.; Chateigner, D.; Lutterotti, L.; Quiros, M.; Serebryanaya, N. R.; Moeck, P.; Downs, R. T.; Le Bail, A., Crystallography Open Database (COD): An Open-Access Collection of Crystal Structures and Platform for World-Wide Collaboration. *Nucleic Acids Res.* **2012**, *40*, D420-D427.
4. Grazulis, S.; Chateigner, D.; Downs, R. T.; Yokochi, A. F. T.; Quiros, M.; Lutterotti, L.; Manakova, E.; Butkus, J.; Moeck, P.; Le Bail, A., Crystallography Open Database - an Open-Access Collection of Crystal Structures. *J. Appl. Crystallogr.* **2009**, *42*, 726-729.
5. Quiros, M.; Grazulis, S.; Girdzijauskaite, S.; Merkys, A.; Vaitkus, A., Using Smiles Strings for the Description of Chemical Connectivity in the Crystallography Open Database. *J. Cheminformatics* **2018**, *10*.
6. Merkys, A.; Vaitkus, A.; Butkus, J.; Okulic-Kazarinas, M.; Kairys, V.; Grazulis, S., *Cod::Cif::Parser*: An Error-Correcting Cif Parser for the Perl Language. *J. Appl. Crystallogr.* **2016**, *49*, 292-301.
7. Downs, R. T.; Hall-Wallace, M., The *American Mineralogist* Crystal Structure Database. *Am. Mineral.* **2003**, *88*, 247-250.
8. Hodges, J. P.; Short, S.; Jorgensen, J. D.; Xiong, X.; Dabrowski, B.; Mini, S. M.; Kimball, C. W., Evolution of Oxygen-Vacancy Ordered Crystal Structures in the Perovskite Series $Sr_nFe_nO_{3n-1}$ (N =

2, 4, 8, and ∞), and the Relationship to Electronic and Magnetic Properties. *J. Solid State Chem.* **2000**, *151*, 190-209.

9. Takeda, Y.; Kanno, K.; Takada, T.; Yamamoto, O.; Takano, M.; Nakayama, N.; Bando, Y., Phase Relation in the Oxygen Nonstoichiometric System, $SrFeO_x$ ($2.5 \leq x \leq 3.0$). *J. Solid State Chem.* **1986**, *63*, 237-249.